

# Many Ways to be Right: Rashomon Sets for Concept-Based Neural Networks

Shihan Feng\*  
Duke University

Cheng Zhang\*  
UNC Chapel Hill

Michael Xi  
Rutgers University

Ethan Hsu  
Duke University

Lesia Semenova  
Rutgers University

Chudi Zhong  
UNC Chapel Hill

## Abstract

*Modern neural networks rarely have a single way to be right. For many tasks, multiple models can achieve identical performance while relying on different features or reasoning patterns, a property known as the Rashomon Effect. However, uncovering this diversity in deep architectures is challenging as their continuous parameter spaces contain countless near-optimal solutions that are numerically distinct but often behaviorally similar. We introduce Rashomon Concept Bottleneck Models, a framework that learns multiple neural networks which are all accurate yet reason through distinct human-understandable concepts. By combining lightweight adapter modules with a diversity-regularized training objective, our method constructs a diverse set of deep concept-based models efficiently without retraining from scratch. The resulting networks provide fundamentally different reasoning processes for the same predictions, revealing how concept reliance and decision making vary across equally performing solutions. Our framework enables systematic exploration of data-driven reasoning diversity in deep models, offering a new mechanism for auditing, comparison, and alignment across equally accurate solutions.*

## 1. Introduction

In many image classification tasks, multiple data-driven explanations can independently justify the same prediction. A bird species, for example, may be identified either by its wing pattern or by the shape of its beak, both of which are semantically meaningful and supported by data. Such diversity in reasoning is inherent to many real-world datasets, yet standard training pipelines produce a single model that shows only one pathway from input to prediction. Under-

standing and capturing alternative but equally valid reasoning routes is important, as it reveals how many different ways a model can be correct, supports more comprehensive auditing, and better aligns with domain expertise.

The Rashomon set framework [37] provides a principled way to study this diversity. A Rashomon set is the collection of models that achieve near-optimal predictive accuracy on a given dataset but behave differently [38, 48]. Prior efforts have constructed Rashomon sets for sparse decision trees [48] and generalized additive models [51] through complete enumeration or convex set approximation, which are tractable due to the structured nature of these hypothesis spaces. However, these techniques do not naturally extend to deep neural networks. Their continuous and high-dimensional parameter spaces can admit infinitely many near-optimal parameterizations obtained through small perturbations. Such variants often differ only numerically while relying on similar underlying reasoning, offering little insight into alternative decision-making processes. Recent work has attempted to explore Rashomon sets for neural networks by varying random seeds in training, applying dropout at inference [19], or perturbing the final linear layer [11], but these approaches either rely on randomness or focus on a small part of the network, leaving the data-driven richness of alternative reasoning pathways largely unexplored.

In this paper, we aim to find multiple neural networks that detect and rely on input signals differently to make correct predictions. We focus on concept-based neural networks [24], as they include an intermediate layer of human-understandable concepts, where a concept encoder first predicts concepts from the input and a classifier then maps concepts to the label. This architecture, commonly referred to as Concept Bottleneck Model (CBM), exposes how concept information is represented and used, enabling direct comparison of reasoning pathways across models. However, existing CBM frameworks are themselves victims of

---

\*Equal contribution.

this single-model paradigm. They are typically optimized to find one fixed mapping from concepts to labels, ignoring that multiple, distinct combinations of concepts could yield the same correct outcome. As a result, these methods produce only a single concept-based model and fail to consider the broader space of distinct but accurate solutions.

We propose Rashomon CBMs, a framework for constructing and analyzing a Rashomon slice (a subset of near-optimal models) of concept-based neural networks. In our architecture, a frozen backbone is shared across models, and small trainable adapter modules are inserted into selected backbone layers to induce variation between models. Each model maintains its own concept-to-label classifier, enabling different mappings from concepts to predictions. We jointly train all models using an objective that minimizes the concept and label prediction losses of the worst-performing model, together with a concept diversity regularizer that encourages learning different concept representations. To make joint training scalable, we introduce a model-axis gradient checkpointing scheme that serializes the backward pass across models, reducing memory usage to nearly that of a single model. Together, these components allow us to efficiently find a meaningful set of diverse yet accurate models with minimal additional training cost.

We evaluate Rashomon CBMs quantitatively and qualitatively on multiple datasets (Awa2, CUB, CIFAR-10, CelebA). Our models maintain competitive accuracy while revealing rich diversity in concept utilization and layer-wise reasoning. Ablation study further shows how adapters influence the diversity. Specifically, our layer-wise eigenvector analysis shows that diversity does not emerge uniformly across layers, but instead concentrates in the adapters of the last few blocks. This pattern reflects a shared low-level structure with increasing model-specific variation at deeper layers in Rashomon CBMs, explaining how they achieve concept diversity while maintaining high accuracy.

Our results demonstrate that Rashomon CBMs bridge interpretability and model multiplicity, providing a concrete pipeline for uncovering the many ways neural networks can reason correctly. By making this diversity explicit and measurable, Rashomon CBMs can help advance the understanding of model behavior while offering practical tools to trust, audit, and align AI systems with human reasoning.

## 2. Related Work

**Rashomon Sets for Neural Networks.** The Rashomon Effect describes that many different models from a function class can explain a dataset almost equally well [4], and the Rashomon set is the collection of these good models [14, 37, 38]. Existing work in this area can be broadly categorized into efforts to compute and characterize the Rashomon Effect and the Rashomon set [10, 19, 48, 51] and efforts that study the implications of the Rashomon set for

different trustworthy applications [2, 3, 16, 32, 39, 42, 45].

For methods exploring Rashomon sets of neural networks, some vary random seeds during training [12], apply dropout at inference [19], or perturb the final layer [11]. Although these approaches produce models with different weights, injected randomness often yields solutions that rely on similar underlying representations, and restricting diversity to the final linear layer probes only a small part of the model space. As a result, these methods offer limited insight into alternative reasoning pathways supported by the data. We aim to find multiple different models that detect and rely on input signals differently.

**Concept Bottleneck Models (CBMs).** CBMs [24] have a special architecture which first predicts concepts from the input and then uses these concepts to predict the label. This two-stage architecture enables users to inspect how concept information is represented and used, and supports human intervention to modify model behavior.

Beyond the standard formulation, recent work explores concept representations by learning richer concept embeddings [13], modeling concept uncertainty [22], capturing dependencies between concepts [43], and disentangling concepts in latent space [7]. Other extensions formulate inference using energy-based objectives to support concept correction and conditional queries [23, 49]. However, these methods focus on producing one single concept-based model without considering the broader space of distinct models that achieve similar accuracy.

**Deep Ensembles.** Deep ensembles train multiple independent networks and average their predictions to improve accuracy, calibration, and out-of-distribution behavior [15, 27, 41]. Among many studies in this field, more closely related to our setting are methods that encourage diversity among ensemble members through explicit regularization [40], specialized ensemble layers [50], or saliency-guided diversity objectives [9]. However, the goal of deep ensembles is fundamentally different from ours. Deep ensembles aggregate multiple models to produce a single improved predictor, and the individual members are not required to be strong or meaningfully different on their own. In contrast, our goal is to find a diverse set of individually accurate models, where each model achieves high performance but relies on distinct internal reasoning. Each model stands on its own, rather than being combined with others.

**Adapters.** Adapters can tune pretrained models by adding small, trainable modules that allow parameter-efficient tuning for downstream tasks. Various adapter designs have been proposed for different backbone architectures [18, 35]. LoRA [21] and its variant [29] are widely used, which injects low-rank matrices into transformer projections. For Vision Transformers, AdaptFormer [6], ViT-Adapter [8], and Conv-Adapter [5] extend adapter designs for dense or spatial tasks with minimal parameters.

Some recent work ensembles multiple LoRA modules attached to a shared backbone to improve performance while remaining parameter-efficient, for example by learning member-specific matrices [33], training multiple mini-LoRA modules [36], combining multiple adapters [1], varying adapter structures [46], or modifying the training process [28]. In this paper, we leverage adapter modules to train multiple diverse models efficiently, where each model independently achieves high accuracy without relying on ensemble aggregation.

### 3. Methods

We first briefly describe concept bottleneck models (CBMs) in general and their training regime and then introduce our method to construct Rashomon CBMs.

Let  $\mathcal{D} = \{\mathbf{x}_i, y_i, \mathbf{c}_i\}_{i=1}^n$  be a dataset, where  $\mathbf{x}_i \in \mathbb{R}^{s_1 \times s_2 \times s_3}$  is an input image,  $y_i \in \{1, \dots, K\}$  is the class label with  $K$  possible classes, and  $\mathbf{c}_i \in \mathbb{R}^p$  is a vector of  $p$  human-interpretable concepts that describe input  $\mathbf{x}_i$ .

#### 3.1. Review of CBMs

A typical CBM consists of a concept encoder  $g(\cdot) : \mathbb{R}^{s_1 \times s_2 \times s_3} \rightarrow \mathbb{R}^p$  that maps input data  $\mathbf{x}$  to a latent concept representation  $\hat{\mathbf{c}} = g(\mathbf{x})$ , and a classifier  $f(\cdot) : \mathbb{R}^p \rightarrow \mathbb{R}$  that maps these concepts to output predictions  $\hat{y} = f(\hat{\mathbf{c}})$ . CBMs jointly optimize for accurate predictions and meaningful concept representations. Let  $\mathcal{L}_c : \mathbb{R}^p \times \mathbb{R}^p \rightarrow \mathbb{R}_{\geq 0}$  be the concept prediction loss, and let  $\mathcal{L}_{\text{pr}} : \mathbb{R} \times \mathbb{R} \rightarrow \mathbb{R}_{\geq 0}$  be the task prediction loss. Usually, binary cross-entropy is used for  $\mathcal{L}_c$ , and cross-entropy for  $\mathcal{L}_{\text{pr}}$ . The CBM is trained by minimizing a joint objective:

$$\mathcal{L}(f, g) = \sum_i \mathcal{L}_{\text{pr}}(f(g(\mathbf{x}_i)), y_i) + \lambda \mathcal{L}_c(g(\mathbf{x}_i), \mathbf{c}_i),$$

where  $\lambda$  controls the tradeoff between concept and task loss.

#### 3.2. Rashomon CBMs framework

We propose a framework for constructing a Rashomon slice of  $M$  concept-based models (CBMs), where each model achieves near-optimal task performance yet relies on concepts in distinct ways, revealing different decision-making logic. A Rashomon slice is a subset of the full Rashomon set (the set of all near-optimal models) restricted to models that satisfy specified design constraints (e.g., the CBM form with a shared backbone and fixed set of concepts). In our framework, each model  $m \in \{1, \dots, M\}$  consists of a concept encoder  $g_m(\cdot)$  and a classifier  $f_m(\cdot)$ , i.e.,  $\hat{y}^{(m)} = f_m(g_m(\mathbf{x}))$ . To construct this Rashomon slice efficiently in both training time and memory usage, all models share a pretrained backbone  $B$  (e.g., ViT or ResNet). The diversity across  $M$  models arises from both the *architecture* and the *diversity loss function*, as described below.

##### 3.2.1. Model Architecture.

We construct  $M$  parallel models by inserting adapter modules into specific layers of a shared backbone network  $B$ . Each model  $m$  maintains its own set of adapters, denoted as  $A_m = \{A_m^{(1)}, A_m^{(2)}, \dots, A_m^{(L)}\}$ , where the superscript indicates the layer index at which an adapter is inserted. During a forward pass, only the adapters associated with model  $m$  are activated, resulting in an effective backbone  $B_m(\mathbf{x}) = B(\mathbf{x}, A_m)$ . The backbone parameters are shared and frozen across all models, while each adapter set  $A_m$  is trainable and model-specific (and thus unique). We denote  $B^{(l)}$  as shared parameters without adapters of layer  $l$ .

Given the adapted features  $B_m(\mathbf{x})$ , each model  $m$  uses a set of per-concept multilayer perceptrons (MLPs)  $\{h_{m,j}\}_{j=1}^p$  to predict the activation of concept  $j$ . The resulting concept prediction vector is then

$$\hat{\mathbf{c}}^{(m)} = g_m(\mathbf{x}) = [h_{m,1}(B_m(\mathbf{x})), \dots, h_{m,p}(B_m(\mathbf{x}))].$$

This design follows Espinosa Zarlenga et al. [13] and Kim et al. [22] to improve the flexibility of learning different concept representations.

Each classifier  $f_m(\cdot)$  then maps the predicted concept vector  $\hat{\mathbf{c}}^{(m)}$  to task label,  $\hat{y}^{(m)} = f_m(\hat{\mathbf{c}}^{(m)})$ . Together, the collection  $\{g_m, f_m\}_{m=1}^M$  forms a data-driven Rashomon slice. Figure 1a summarizes the proposed architecture.

##### 3.2.2. Loss function.

To obtain multiple distinct yet well-performing models, we jointly optimize all  $M$  models using a customized loss that combines task prediction loss, concept loss, and diversity among models regularization, i.e.,

$$\mathcal{L}_{\text{total}} = \max_m \mathcal{L}_{\text{pr}}^{(m)} + \lambda \left( \max_m \mathcal{L}_c^{(m)} - \frac{\alpha}{M} \sum_{m=1}^M \mathcal{L}_{\text{div}}^{(m)} \right). \quad (1)$$

Both  $\mathcal{L}_{\text{pr}}^{(m)}$  and  $\mathcal{L}_c^{(m)}$  follow the definitions in Section 3.1. We penalize the maximum prediction and concept losses across models to keep all models accurate. The average diversity loss is used to encourage models to learn different concept representations. For each model  $m$ , a diversity loss is defined as  $\mathcal{L}_{\text{div}}^{(m)} = 1 - \frac{1}{M-1} \sum_{m' \neq m} \text{sim}(m, m')$ , where  $\text{sim}(\cdot, \cdot)$  is the cosine similarity between predicted concept vectors in model  $m$  and  $m'$ .

In Eq (1),  $\lambda$  controls the contribution from concept-related objectives, and  $\alpha$  corresponds to the strength of diversity regularization. Together, this formulation prevents any model from collapsing while encouraging useful diversity among concept pathways.

Inspired by Zhang et al. [50], we update  $\alpha$  dynamically during training based on gradient magnitude, i.e.,

$$\alpha^{(t+1)} = \sigma \left( \mathbb{E}_{w \in \mathcal{P}} \left[ \overline{|\nabla_w \mathcal{L}_{\text{total}}^{(t)}|} \right] \right),$$

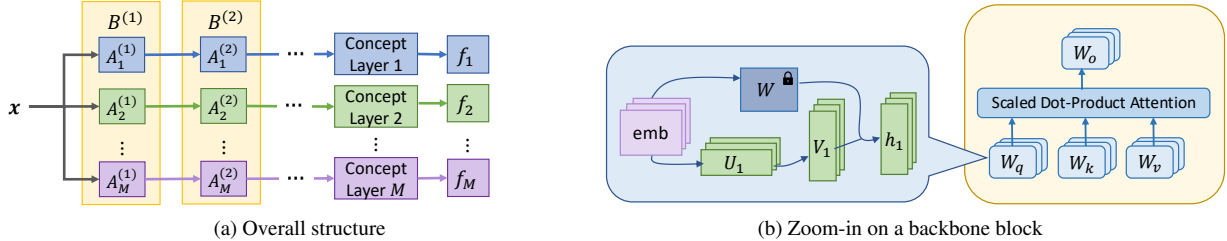


Figure 1. Proposed architecture for Rashomon CBMs. (a) Overall structure: an input image passes through a frozen backbone with attached adapters, followed by multiple parallel concept layers, each linked to a classifier. (b) Zoom-in on a backbone block: at each Attention layer, multiple adapter modules are inserted in parallel into the Q, K, V, and projection mappings, operating concurrently and independently. All adapters are trained jointly, while at inference, each model activates only its own adapters while sharing the same backbone weights.

where  $\mathcal{P}$  denotes all parameters in the concept heads and  $|\cdot|$  is the average of absolute values in the tensor. Early in training,  $\alpha$  is usually close to 1 and gradually decreases as optimization converges. Since we freeze the pretrained backbone, gradient magnitudes are relatively smaller, and the initial  $\alpha$  is around 0.5 – 0.6.

### 3.2.3. Instantiation with ViT and Adapters.

Though the proposed Rashomon architecture is backbone- and adapter-agnostic, we illustrate it using a Vision Transformer (ViT) backbone with Low-Rank Adaptation (LoRA) modules as an example. Each model  $m$  is equipped with its own set of LoRA modules inserted into the self-attention projections of every transformer block. As in Hu et al. [21], for a pretrained weight matrix  $W \in \mathbb{R}^{d_{out} \times d_{in}}$  where  $d_{in}$  and  $d_{out}$  are input and output feature dimensions respectively, we constrain its update by representing the latter with a low-rank decomposition  $W + \Delta W = W + UV$ , where  $U \in \mathbb{R}^{d_{out} \times r}$ ,  $V \in \mathbb{R}^{r \times d_{in}}$  and the rank  $r \ll \min(d_{in}, d_{out})$ . An optional dropout can be applied during training to regularize the low-rank updates. While the formulation illustrates a single weight matrix, each model  $m$  applies this low-rank update scheme to multiple projection matrices across transformer blocks in the backbone. Together, the resulting set of LoRA parameters  $\{U_m^{(l)}, V_m^{(l)}\}$  constitutes the adapter set  $A_m$  that differentiates model  $m$  from other members of the Rashomon slice (see Figure 1b).

### 3.2.4. Model-axis checkpointing scheme for efficient memory usage.

To further improve memory efficiency during joint Rashomon training, we extend gradient checkpointing beyond its conventional use within a single model. Standard checkpointing operates along the model’s layer-axis, interleaving forward-and-checkpoint operations across the layers of the network, thereby reducing memory by reclaiming activations at the cost of extra recomputation. In our setup of  $M$  models, performing layer-wise checkpointing individually for each model would require holding partial activations or recomputing for all  $M$  forward passes in parallel,

causing memory usage to scale roughly linearly with  $M$ . To avoid this blow-up, we introduce a *model-axis checkpointing scheme*. That is, we wrap each model’s full forward (and backward) invocation inside a checkpoint boundary, such that only one model is active and holds its activations at any given time during the backward pass. It proves to be especially useful when  $M$  is large, but GPU memory is limited. Empirically, we observed that this approach allows training and backpropagation across the full Rashomon slice with memory usage comparable to those of a single model, instead of the linear memory growth that would otherwise occur with standard checkpointing.

## 4. Experiments

Our evaluation answers the following questions: (1) How do Rashomon CBMs compare to baseline methods in discovering diverse yet well-performing models? (2) How does the number of models influence the diversity and accuracy? (3) Where does diversity emerge within the network, and how does it evolve across layers? (4) How do Rashomon CBMs behave under different backbones? (5) What qualitative differences arise in how individual models rely on concepts?

### 4.1. Experimental setup

**Datasets.** We conduct experiments on four widely used benchmark datasets: CUB-200-2011 [44], Awa2 [47], CIFAR-10 [26], and CelebA [30]. These datasets span fine-grained and coarse-grained visual domains, enabling a comprehensive assessment of our method. For datasets with human-annotated concepts (CUB and Awa2), we directly adopt their provided concept annotations and category labels for CBM training. For CIFAR-10, which lacks explicit concept annotations, we follow the automatic concept discovery pipeline proposed in Oikarinen et al. [34], where a pretrained CLIP model is used to generate concept labels aligned with visual and textual semantics. For CelebA, following Espinosa Zarlenga et al. [13], we select the eight most balanced facial attributes and use them to construct

	Metric	random init	dropout	c2y	x2c	Rashomon CBMs (Ours)
CIFAR-10	concept acc $\uparrow$	<b>0.8905 <math>\pm</math> 0.0005</b>	0.8813 $\pm$ 0.0005	0.8894 $\pm$ 0.0005	0.8877 $\pm$ 0.0006	0.8840 $\pm$ 0.0010
	task acc $\uparrow$	0.9763 $\pm$ 0.0012	0.9595 $\pm$ 0.0012	0.9766 $\pm$ 0.0015	0.9760 $\pm$ 0.0004	<b>0.9811 <math>\pm</math> 0.0011</b>
	pred hamming $\uparrow$	0.0256 $\pm$ 0.0042	<b>0.0265 <math>\pm</math> 0.0012</b>	0.0032 $\pm$ 0.0006	0.0222 $\pm$ 0.0009	0.0133 $\pm$ 0.0010
	concept cka $\downarrow$	0.9428 $\pm$ 0.0058	1.0000 $\pm$ 0.0000	-	0.3159 $\pm$ 0.1188	<b>0.2364 <math>\pm</math> 0.1728</b>
	SHAP Sim $\downarrow$	0.7663 $\pm$ 0.0503	0.9941 $\pm$ 0.0007	0.9074 $\pm$ 0.0240	0.0909 $\pm$ 0.1158	<b>0.0318 <math>\pm</math> 0.0074</b>
	union size $\uparrow$	36	15	19	<b>53</b>	49
AWA2	concept acc $\uparrow$	0.9795 $\pm$ 0.0010	0.9764 $\pm$ 0.0008	0.9834 $\pm$ 0.0002	0.9818 $\pm$ 0.0009	<b>0.9885 <math>\pm</math> 0.0008</b>
	task acc $\uparrow$	0.9312 $\pm$ 0.0024	0.9138 $\pm$ 0.0043	0.9292 $\pm$ 0.0012	0.9259 $\pm$ 0.0044	<b>0.9624 <math>\pm</math> 0.0030</b>
	pred hamming $\uparrow$	0.0762 $\pm$ 0.0045	0.0608 $\pm$ 0.0024	0.0149 $\pm$ 0.0013	<b>0.0791 <math>\pm</math> 0.0045</b>	0.0269 $\pm$ 0.0015
	concept cka $\downarrow$	0.9222 $\pm$ 0.0038	0.9936 $\pm$ 0.0020	-	0.3568 $\pm$ 0.1013	<b>0.3371 <math>\pm</math> 0.1462</b>
	SHAP Sim $\downarrow$	0.9343 $\pm$ 0.0084	0.9990 $\pm$ 0.0001	0.9753 $\pm$ 0.0037	<b>0.1560 <math>\pm</math> 0.0878</b>	0.2046 $\pm$ 0.0576
	union size $\uparrow$	43	19	33	<b>67</b>	59

Table 1. Comparison of Rashomon CBMs and baseline methods on the CIFAR-10 and AWA2 datasets. All methods achieve comparable concept and task accuracies on the test set. Our method consistently achieves better concept representation and SHAP diversity than baselines, and performs on par with or better than x2c, indicating that Rashomon CBMs effectively enumerate diverse yet well-performing solutions within the model space. Best results per metric are highlighted in bold.

both concept and task supervision: the first six attributes serve as binary concepts, while all eight together define  $2^8 = 256$  composite classes. This formulation ensures that the dataset admits a structured concept space while maintaining sufficient label diversity.

**Baselines.** We systematically compare the performance of our method against four baseline models, including random initialization, dropout CBMs, a baseline that has separate concept encoders denoted as x2c, and a baseline that is similar to Zhang et al. [50] and shares one concept encoder but differs in classifiers, denoted as c2y.

- *Random initialization* is a common way for training a collection of models. We train  $M$  CBMs using different random seeds for parameter initialization. Each CBM is fully tunable, with all parameters updated during training.
- *Dropout CBMs* adopts a simple stochastic scheme to approximate a Rashomon set without retraining multiple models. Following Hsu et al. [20], we insert dropout layers throughout the backbone and train a single CBM with dropout enabled. At inference time, we keep dropout active and resample the mask by varying and freezing the random seed, so each dropout pattern produces a distinct stochastic instantiation of the same trained CBM.
- *c2y* follows Zhang et al. [50] and can be viewed as a variant of a deep ensemble. It uses a shared, fully tunable backbone  $B$  and a shared concept predictor  $g$ , while each model maintains its own task classifier  $f_m$ . All models are trained jointly, and the diversity regularization term is applied at the task prediction level.
- *x2c* is similar to the random initialization setup, where each model is given its own fully-trainable backbone and classifiers. However, unlike random initialization, we enable joint training across models, and the diversity regu-

	random	c2y	x2c	Ours	
ViT	Mem (GB)	37.09	3.75	37.09	<b>2.88</b>
	Mem ratio (%)	-	10.1%	100%	<b>7.6%</b>
	# Params (millions)	217.2	21.7	217.2	<b>2.9</b>
	# Params ratio (%)	-	10.0%	100%	<b>1.3%</b>

Table 2. Exact and relative memory and parameter costs on CIFAR-10 using ViT backbone. Random initialization serves as the baseline for ratios. Our method achieves strong diversity with substantially lower memory and parameter cost than baselines.

larization is applied at the concept level.

**Metrics.** We evaluate all methods using both concept prediction accuracy and label classification accuracy. Beyond accuracy, we report a set of diversity metrics that provide a more comprehensive analysis of how models differ. Our comparisons are organized into three groups of metrics that measure diversity (a) in label predictions, (b) in concept predictions, and (c) in concept utilization for decision making.

- *Prediction hamming distance* measures the fraction of test samples on which two models make different predictions. It quantifies output-level diversity, where higher values indicate greater disagreement.
- Following Kornblith et al. [25], *Centered Kernel Alignment (CKA)* compares the concept representations of two models. Using a linear kernel  $k(\mathbf{x}, \mathbf{y}) = \mathbf{x}^\top \mathbf{y}$ , we form Gram matrices  $K^{(m_1)}$  and  $K^{(m_2)}$  from the two models’ concept representations evaluated on the same inputs, center them as  $\tilde{K}^{(m)} = HK^{(m)}H$  with  $H = I - \frac{1}{n}\mathbf{1}\mathbf{1}^\top$ . CKA is then computed as the cosine similarity between these centered Gram matrices, normalized by their Frobenius norms. Higher CKA indicates more similar concept

representations.

- *SHAP similarity* [31] measures how similarly different models use learned concepts for prediction. We obtain SHAP importance scores over concepts for each model, forming a SHAP importance vector. Diversity is measured by the cosine similarity between the SHAP vectors of two models, where lower similarity indicates more distinct usage of concepts for decision-making.

For each metric, we compute all pairwise scores across models to form an  $M \times M$  similarity matrix  $S$  on a fixed test set. We summarize diversity using the off-diagonal mean  $\bar{S}_{\text{off}} = \frac{2}{M(M-1)} \sum_{m_1 < m_2} S_{m_1 m_2}$ , where a higher value indicates stronger agreement among models except for prediction hamming distance. Additionally, for each model, we rank concepts by its SHAP importance scores and select its top 10, and then report the size of the union of these top-10 sets across models. The size quantifies how much the models’ most influential concepts overlap. A larger union indicates more diverse concept usage.

**ViT backbone implementation details.** For all ViT experiments, we adopt pretrained ViT-S/16 as the backbone. We instantiate our proposed framework using LoRA adapters. Each LoRA module is inserted into the  $Q$ ,  $K$ ,  $V$ , and projection matrices of every attention block, with a rank of  $r = 8$ , scaling factor  $\alpha = 16$ , and 0.1 dropout ratio. All backbones are frozen, and only the adapter parameters and concept heads are updated during training. Models are trained using the Adam optimizer with a learning rate of  $1 \times 10^{-4}$ , batch size of 64, and no weight decay for 500 epochs. We stop training early if the validation loss doesn’t decrease for 30 epochs. For most datasets,  $\lambda = 1$  yields stable accuracy and diversity. For the CUB dataset, it is set to 4 to ensure diversity. Training is performed on a single NVIDIA L40 GPU (48GB) for all ViT results. For all methods, the concept predictor  $\{h_{m,j}\}_{j=1}^p$  and label classifier  $f_m$  are implemented as linear layers.

## 4.2. Rashomon CBMs learn diverse models

In this section, we show the performance of our Rashomon CBMs with ViT instantiation. We report results for the Rashomon slices of size  $M = 10$ . Table 1 compares performance across different methods on CIFAR-10 and Awa2 datasets. All methods achieve comparable concept and task accuracies on the test set (within  $\sim 2\%$ ). With a similar level of accuracy, Rashomon CBMs have better concept and SHAP diversity, performing on par with or better than the most complex baseline x2c. Similar trends are observed on CUB and CelebA datasets (see Table 4 in Appendix A.1).

We also report the memory cost and the number of trainable parameters for each method on CIFAR-10 dataset with ViT backbone in Table 2. Rashomon CBMs achieve better diversity while using only 7.6% of the memory and 1.3% of

Metric	random init	x2c	Our Model
concept acc $\uparrow$	96.92 $\pm$ 0.09	<b>97.63 <math>\pm</math> 0.08</b>	95.08 $\pm$ 0.50
task acc $\uparrow$	90.07 $\pm$ 0.61	90.96 $\pm$ 0.41	<b>91.92 <math>\pm</math> 0.48</b>
pred hamming $\uparrow$	<b>0.092 <math>\pm</math> 0.006</b>	0.079 $\pm$ 0.002	0.046 $\pm$ 0.003
concept cka $\downarrow$	0.924 $\pm$ 0.008	<b>0.349 <math>\pm</math> 0.106</b>	0.674 $\pm$ 0.175
SHAP sim $\downarrow$	0.955 $\pm$ 0.006	0.130 $\pm$ 0.058	<b>0.112 <math>\pm</math> 0.084</b>
union size $\uparrow$	41	<b>63</b>	58

Table 3. Comparison of performance on the Awa2 dataset with a ResNet-18 backbone. Rashomon CBMs achieve the highest task accuracy and competitive diversity. Best per metric in bold.

the trainable parameters required by random initialization and x2c. This substantial reduction stems from our adapter-based tuning and model-axis checkpointing schema, which activates one model at a time during backpropagation, avoiding the linear memory growth across  $M$  models inherent in standard layer-wise checkpointing. As a result, the entire Rashomon slice can be trained at a memory cost comparable to that of a single model, demonstrating excellent efficiency and scalability. Although x2c can sometimes achieve slightly better diversity, it requires 70 $\times$  more parameters, making it less practical for large scale applications. More results are in Appendix A.1.

## 4.3. Rashomon CBMs generalize to different backbones

As discussed in Section 3.2, our design is backbone-agnostic. Here, we demonstrate that it generalizes effectively across architectures, achieving strong performance under a ResNet-18 backbone. For ResNet-18, the architecture is convolutional, so we replace the LoRA with Conv-Adapter [5]. To construct a Rashomon slice of  $M$  models, we augment each convolutional layer with  $M$  parallel Conv-Adapters. Then the output of the convolutional layer is combined with the output of each adapter, producing  $M$  parallel feature streams that are fed into the next layer. In this way, each model  $m$  has its own dedicated sequence of adapters, with no sharing of adapters across models, while the backbone weights remain shared and frozen. For baselines, we also use ResNet-18 as the backbone. Training configurations can be found in Section A.2 in Appendix.

Table 3 compares performance across different methods on Awa2 dataset. Rashomon CBMs achieve the highest task accuracy, while maintaining diversity in prediction, concept representation, and reliance comparable to x2c. Rashomon CBMs substantially outperform the random initialization baseline. We provide more results for ResNet-18 backbone in Appendix A.2.

## 4.4. Scalability of Rashomon CBMs

Our framework scales efficiently, enabling systematic exploration of the innate diversity captured by the Rashomon

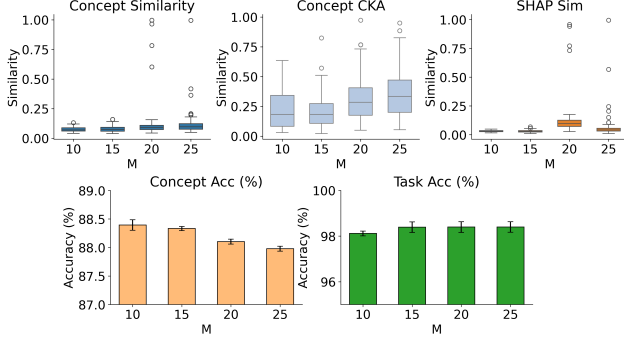


Figure 2. Effect of varying the number of models ( $M$ ) from 10 to 25 on accuracy and diversity on CIFAR-10. As  $M$  increases, concept similarity and CKA rise while concept accuracy decreases slightly, indicating mild convergence in the representation space.

slice across different datasets. Due to its memory-efficient design, we can expand the Rashomon slice by increasing the number of models  $M$  without exceeding GPU limits. We vary  $M$  from 10 to 25 on CIFAR-10 and examine how accuracy and pairwise diversity evolve as the slice grows (similar results for CUB are in Appendix C).

As shown in Figure 2, expanding the Rashomon slice does not lower the task accuracy. For CIFAR-10, the models within the slice exhibit slightly higher CKA similarity at larger  $M$ , suggesting mild convergence in representation space. In contrast, on CUB, the average task accuracy and SHAP similarity across models in Rashomon slice remains stable even at  $M=25$  (see Appendix C), illustrating that our approach can capture a large and diverse Rashomon slice when the underlying data supports it. Overall, these findings demonstrate that our architecture is highly scalable and reveal how the effective Rashomon slice size is shaped by the intrinsic diversity of the dataset. Future work may further quantify this size limit, for example, through model merging techniques [17].

#### 4.5. Adapters lead to different concept reliances

With the backbone frozen and shared, architectural diversity in our framework comes from the LoRA adapters and final linear heads. To localize the source of this diversity, we follow Mühlematter et al. [33] and quantify weight-space variation via Singular Value Decomposition (SVD). For each transformer block, we compute the cosine similarity between the top-16 right singular vectors of the LoRA-augmented value projection matrices across Rashomon slice members. We perform this analysis for the query, key, and output projection matrices. As shown in Figure 3, the leading directions in early layers remain strongly aligned across models, while similarity gradually declines with depth and diversity concentrates in the adapters of the final few blocks. This means that models

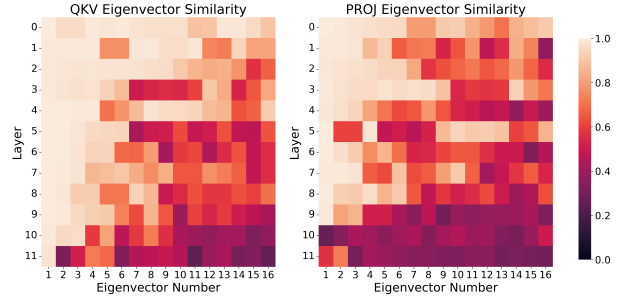


Figure 3. Layerwise eigenvector similarity on QKV matrices (left) and projection matrices (right) between models sharing the same ViT backbone on AwA2. Similarity gradually declines with depth, and diversity concentrates in the adapters of the final few blocks.

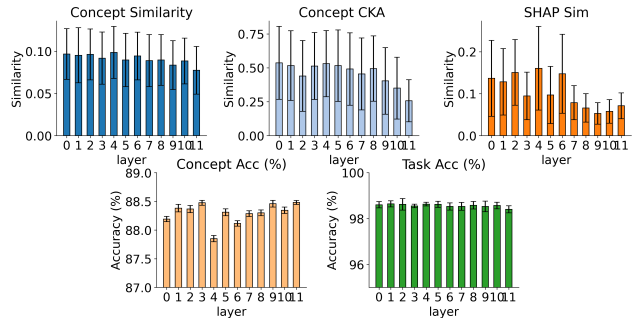


Figure 4. Layerwise ablation analysis on CIFAR-10 with a ViT backbone. Adapters in each layer are switched from shared to independent one at a time. Task accuracy remains stable, while similarity metrics decrease as deeper layers become independent.

can learn low-level concepts in the same way, but diverge when learning higher-level concepts, which explains why our framework can achieve a good balance between accuracy and diversity. More results are in Appendix B.1.

While this eigenvector analysis asks where the models naturally diversify when every layer is free to differ, we next consider another question: if architectural independence is restricted to a single layer, where is it most effective for inducing diversity in concept space? To explore this, we conduct a layer-wise ablation in which we selectively decouple LoRA modules across models. Starting from a configuration where all adapters are shared across Rashomon slice members, we independently train only one layer’s adapters at a time. Specifically, for each layer index  $\ell \in \{0, \dots, L - 1\}$ , we let the adapters  $\{A_m^{(\ell)}\}_{m=1}^M$  be trained independently for each member, while all other layers remain shared as a common  $A^{(k)}$  ( $k \neq \ell$ ). We retrain under each configuration and track both accuracy and cross-model similarity. Figure 4 shows that, for CIFAR-10, adapters in the deep layers tend to produce more diversity with minor changes in accuracy. This trend implies that

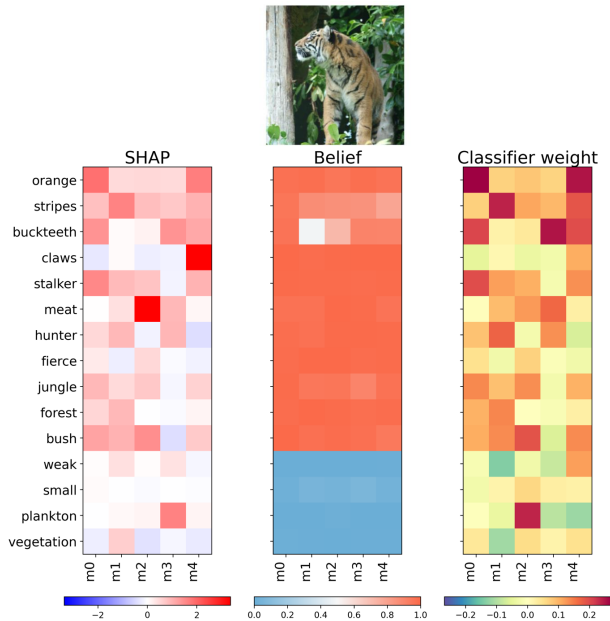


Figure 5. Qualitative Analysis of Rashomon CBMs on a tiger image from Awa2 dataset. The left heatmap shows sparse SHAP importance for 5 models, indicating each model relies on different concepts for prediction. The middle heatmap shows the predicted concept probabilities, which are quite consistent across models. The right heatmap visualizes the linear classifier weights assigned to each concept, suggesting that the models differ in how they map concepts to final predictions.

later layers may have a stronger influence on representational diversity. Note that similar to Figure 4 top mid plot, we observe a slight decrease in the concept CKA metric as layers are switched from shared to independent across different architectures and datasets (see the Appendix C for more details).

#### 4.6. Qualitative results

To qualitatively illustrate how our method achieves diversity, we visualize how models predict and use concepts. Specifically, we visualize SHAP values, predicted concept probability for each model, and weights assigned to each concept (recall that  $f_m$  is linear). We manually pick 15 concepts that fall in four categories: visual, behavioral, environmental, and negative traits. Figure 5 shows a representative example. It was learned with  $M = 10$  and we show 5 models out of 10 (see Figure 9 for all 10 models and more concepts and Appendix D for more qualitative examples).

From the SHAP and classifier-weight heatmaps, we observe that different models rely on noticeably different combinations of concepts: some put most of their positive mass on visual concepts such as “orange” and “stripes”, others emphasize semantic and behavioral characters like “stalker” and “meat”, or even contextual cues such as “jungle” and

“bush”. At the same time, the rows of the heatmaps reveal clear points of agreement: concepts like “orange”, “stripes” and “stalker” consistently obtain high positive values across many models, indicating that the models have discovered a set of canonical tiger-like concepts.

The belief heatmap explains why this diversity does not hurt and, in fact, supports accurate predictions. For most concepts that are truly present in the image, the models assign high belief values, while clearly non-tiger concepts receive uniformly low belief. Thus, although each model combines concepts differently, they all reason within a largely correct concept space.

Finally, the three heatmaps together show that Rashomon slice members learn tiger from complementary angles. Model 0 mainly relies on visual concepts such as coat color and shape. It assigns high belief and positive weights to “orange”, “buckteeth” and “stalker”, and also uses “jungle”, “bush” and “forest”, so it sees tigers as “orange stalkers moving through woods”. Model 1 focuses on visual and behavioral features like “stripes” and “hunter”, while also learning what a tiger is not by giving negative weights to “weak” and “vegetation”. Model 2 emphasizes predatory behavior and the surrounding environment. The concept “meat” dominates its SHAP values, with “bush” and “jungle” only playing a supporting role. This model differs from others, and its reliance on “meat” likely reflects properties of the dataset (e.g. tiger images often co-occur with predatory cues and “meat” helps differentiate the tiger from other classes like sheep and beaver). Here, the classifier places relatively large weight on “plankton” (most likely due to correlation with greenery), but its low belief prevent it from driving the prediction. SHAP value is also small. Model 3 combines positive behavioral evidence from “buckteeth”, “meat” and “hunter” with non-tiger traits. In the right two plots, “plankton” has a negative weight and low belief. But in the SHAP plot, it shows a strong positive contribution. This discrepancy is likely due to the local approximate nature of SHAP or correlation with other greenery-related concepts in the image. Model 4 centers its decision on visual characteristics of tigers, with large positive SHAP on “orange” and “claws”. Meanwhile, it also learns from what a tiger is not by using concepts such as “plankton” negatively. Overall, the slice of models spans visual appearance, predatory behavior, background context and exclusion of non-tiger attributes, providing a rich but human-interpretable set of ways in which “tiger” can be represented, allowing for better choice of model depending on the domain needs.

#### 5. Conclusions

This work introduced Rashomon Concept Bottleneck Models (Rashomon CBMs), a new lightweight framework for systematically computing the multiplicity of

equally-accurate-yet-conceptually-distinct neural networks. Beyond their immediate empirical performance, the Rashomon CBMs open several directions for understanding and leveraging model diversity. Because each member of the Rashomon slice exposes a distinct, interpretable mapping from concepts to predictions, practitioners can now inspect *how and why* multiple valid reasoning strategies emerge within the same task. This perspective enables both auditing (by identifying models that depend on spurious correlations) and alignment (by selecting models that best match human or domain-specific reasoning). The ability to visualize concept reliance and feature attributions across the Rashomon slice could also facilitate interactive exploration tools, where users inspect the “many ways to be right” and decide which reasoning style to deploy in safety-critical or socially sensitive settings.

## References

- [1] Yue Bai, Handong Zhao, Zhe Lin, Ajinkya Kale, Jiuxiang Gu, Tong Yu, Sungchul Kim, and Yun Fu. Advancing vision-language models with adapter ensemble strategies. In *Findings of the Association for Computational Linguistics: EMNLP 2024*, pages 15702–15720, 2024. 3
- [2] Emily Black, Manish Raghavan, and Solon Barocas. Model multiplicity: Opportunities, concerns, and solutions. In *2022 ACM Conference on Fairness, Accountability, and Transparency*, pages 850–863, 2022. 2
- [3] Zachery Boner, Harry Chen, Lesia Semenova, Ronald Parr, and Cynthia Rudin. Using noise to infer aspects of simplicity without learning. *Advances in Neural Information Processing Systems*, 37:131824–131858, 2024. 2
- [4] Leo Breiman. Statistical modeling: The two cultures (with comments and a rejoinder by the author). *Statistical science*, 16(3):199–231, 2001. 2
- [5] Hao Chen, Ran Tao, Han Zhang, Yidong Wang, Weirong Ye, Jindong Wang, Guosheng Hu, and Marios Savvides. Conv-adapter: Exploring parameter efficient transfer learning for convnets. *2024 IEEE/CVF Conference on Computer Vision and Pattern Recognition Workshops (CVPRW)*, pages 1551–1561, 2022. 2, 6
- [6] Shoufa Chen, Chongjian Ge, Zhan Tong, Jiangliu Wang, Yibing Song, Jue Wang, and Ping Luo. Adaptformer: Adapting vision transformers for scalable visual recognition. *ArXiv*, abs/2205.13535, 2022. 2
- [7] Zhi Chen, Yijie Bei, and Cynthia Rudin. Concept whitening for interpretable image recognition. *Nature Machine Intelligence*, 2(12):772–782, 2020. 2
- [8] Zhe Chen, Yuchen Duan, Wenhai Wang, Junjun He, Tong Lu, Jifeng Dai, and Y. Qiao. Vision transformer adapter for dense predictions. *ArXiv*, abs/2205.08534, 2022. 2
- [9] Stanislav Dereka, Ivan Karpukhin, Maksim Zhdanov, and Sergey Kolesnikov. Diversifying deep ensembles: A saliency map approach for enhanced ood detection, calibration, and accuracy. In *2024 IEEE International Conference on Image Processing (ICIP)*, pages 437–443, 2024. 2
- [10] Jiayun Dong and Cynthia Rudin. Exploring the cloud of variable importance for the set of all good models. *Nature Machine Intelligence*, 2(12):810–824, 2020. 2
- [11] Jon Donnelly, Zhicheng Guo, Alina Jade Barnett, Hayden McTavish, Chaofan Chen, and Cynthia Rudin. Rashomon sets for prototypical-part networks: Editing interpretable models in real-time. In *Proceedings of the Computer Vision and Pattern Recognition Conference*, pages 4528–4538, 2025. 1, 2
- [12] Alexander D’Amour, Katherine Heller, Dan Moldovan, Ben Adlam, Babak Alipanahi, Alex Beutel, Christina Chen, Jonathan Deaton, Jacob Eisenstein, Matthew D Hoffman, et al. Underspecification presents challenges for credibility in modern machine learning. *Journal of Machine Learning Research*, 2020. 2
- [13] Mateo Espinosa Zarlenga, Pietro Barbiero, Gabriele Ciravegna, Giuseppe Marra, Francesco Giannini, Michelangelo Diligenti, Zohreh Shams, Frederic Precioso, Stefano Melacci, Adrian Weller, et al. Concept embedding models: Beyond the accuracy-explainability trade-off. *Advances in neural information processing systems*, 35:21400–21413, 2022. 2, 3, 4
- [14] Aaron Fisher, Cynthia Rudin, and Francesca Dominici. All models are wrong, but many are useful: Learning a variable’s importance by studying an entire class of prediction models simultaneously. *Journal of Machine Learning Research*, 20(177):1–81, 2019. 2
- [15] Stanislav Fort, Huiyi Hu, and Balaji Lakshminarayanan. Deep ensembles: A loss landscape perspective. *ArXiv*, abs/1912.02757, 2019. 2
- [16] Prakhar Ganesh, Afaf Taik, and Golnoosh Farnadi. The curious case of arbitrariness in machine learning. *arXiv preprint arXiv:2501.14959*, 2025. 2
- [17] Shwai He, Run-Ze Fan, Liang Ding, Li Shen, Tianyi Zhou, and Dacheng Tao. Merging experts into one: Improving computational efficiency of mixture of experts. *ArXiv*, abs/2310.09832, 2023. 7
- [18] Neil Houlsby, Andrei Giurgiu, Stanislaw Jastrzebski, Brianna Morrone, Quentin De Laroussilhe, Andrea Gesmundo, Mona Attariyan, and Sylvain Gelly. Parameter-efficient transfer learning for NLP. In *International Conference on Machine Learning (ICML)*, 2019. 2
- [19] Hsiang Hsu and Flavio Calmon. Rashomon capacity: A metric for predictive multiplicity in classification. In *Neural Information Processing Systems (NeurIPS)*, pages 28988–29000, 2022. 1, 2
- [20] Hsiang Hsu, Guihong Li, Shaohan Hu, and Chun-Fu Chen. Dropout-based rashomon set exploration for efficient predictive multiplicity estimation. In *International Conference on Representation Learning*, pages 33104–33144, 2024. 5
- [21] Edward J Hu, Phillip Wallis, Zeyuan Allen-Zhu, Yuanzhi Li, Shean Wang, Lu Wang, Weizhu Chen, et al. Lora: Low-rank adaptation of large language models. In *International Conference on Learning Representations*, 2022. 2, 4
- [22] Eunji Kim, Dahuin Jung, Sangha Park, Siwon Kim, and Sungroh Yoon. Probabilistic concept bottleneck models. In *Proceedings of the 40th International Conference on Machine Learning (ICML)*. JMLR.org, 2023. 2, 3

- [23] Sangwon Kim, Dasom Ahn, Byoung Chul Ko, In su Jang, and Kwang-Ju Kim. Eq-cbm: A probabilistic concept bottleneck with energy-based models and quantized vectors, 2024. 2
- [24] Pang Wei Koh, Thao Nguyen, Yew Siang Tang, Stephen Mussmann, Emma Pierson, Been Kim, and Percy Liang. Concept bottleneck models. In *International conference on machine learning*, pages 5338–5348. PMLR, 2020. 1, 2
- [25] Simon Kornblith, Mohammad Norouzi, Honglak Lee, and Geoffrey Hinton. Similarity of neural network representations revisited. In *International conference on machine learning*, pages 3519–3529. PMIR, 2019. 5
- [26] Alex Krizhevsky. Learning multiple layers of features from tiny images. Technical Report TR-2009, University of Toronto, 2009. 4
- [27] Balaji Lakshminarayanan, Alexander Pritzel, and Charles Blundell. Simple and scalable predictive uncertainty estimation using deep ensembles. In *Neural Information Processing Systems*, 2016. 2
- [28] Yinghao Li, Vianne Gao, Chao Zhang, and MohamadAli Torkamani. Ensembles of low-rank expert adapters. *arXiv preprint arXiv:2502.00089*, 2025. 3
- [29] Shih-Yang Liu, Chien-Yi Wang, Hongxu Yin, Pavlo Molchanov, Yu-Chiang Frank Wang, Kwang-Ting Cheng, and Min-Hung Chen. Dora: Weight-decomposed low-rank adaptation. *ArXiv*, abs/2402.09353, 2024. 2
- [30] Ziwei Liu, Ping Luo, Xiaogang Wang, and Xiaoou Tang. Deep learning face attributes in the wild. In *Proceedings of International Conference on Computer Vision (ICCV)*, 2015. 4
- [31] Scott M Lundberg and Su-In Lee. A unified approach to interpreting model predictions. *Advances in neural information processing systems*, 30, 2017. 6
- [32] Charles Marx, Flavio Calmon, and Berk Ustun. Predictive multiplicity in classification. In *Proceedings of the International Conference on Machine Learning (ICML)*, pages 6765–6774, 2020. 2
- [33] Dominik J Mühlematter, Michelle Halbheer, Alexander Becker, Dominik Narnhofer, Helge Aasen, Konrad Schindler, and Mehmet Ozgur Turkoglu. Lora-ensemble: Efficient uncertainty modelling for self-attention networks. *arXiv preprint arXiv:2405.14438*, 2024. 3, 7
- [34] Tuomas P. Oikarinen, Subhro Das, Lam M. Nguyen, and Tsui-Wei Weng. Label-free concept bottleneck models. *ArXiv*, abs/2304.06129, 2023. 4
- [35] Sylvestre-Alvise Rebuffi, Hakan Bilen, and Andrea Vedaldi. Learning multiple visual domains with residual adapters. In *Advances in Neural Information Processing Systems (NeurIPS)*, 2017. 2
- [36] Pengjie Ren, Chengshun Shi, Shiguang Wu, Mengqi Zhang, Zhaochun Ren, Maarten de Rijke, Zhumin Chen, and Jiahuan Pei. Melora: Mini-ensemble low-rank adapters for parameter-efficient fine-tuning. *arXiv preprint arXiv:2402.17263*, 2024. 3
- [37] Cynthia Rudin, Chudi Zhong, Lesia Semenova, Margo Seltzer, Ronald Parr, Jiachang Liu, Srikar Katta, Jon Donnelly, Harry Chen, and Zachery Boner. Amazing things come from having many good models. In *Proceedings of the International Conference on Machine Learning (ICML)*, 2024. 1, 2
- [38] Lesia Semenova, Cynthia Rudin, and Ronald Parr. On the existence of simpler machine learning models. In *ACM Conference on Fairness, Accountability, and Transparency (ACM FAccT)*, 2022. 1, 2
- [39] Lesia Semenova, Harry Chen, Ronald Parr, and Cynthia Rudin. A path to simpler models starts with noise. *Advances in neural information processing systems*, 36:3362–3401, 2023. 2
- [40] Changjian Shui, Azadeh Sadat Mozafari, Jonathan Marek, Ihsen Hedhli, and Christian Gagné. Diversity regularization in deep ensembles. *ArXiv*, abs/1802.07881, 2018. 2
- [41] Asa Cooper Stickland and Iain Murray. Diverse ensembles improve calibration. *ArXiv*, abs/2007.04206, 2020. 2
- [42] Bohdan Turbal, Iryna Voitsitska, and Lesia Semenova. ELICE: Efficient and provably robust algorithmic recourse via the rashomon sets. In *The Thirty-ninth Annual Conference on Neural Information Processing Systems*, 2025. 2
- [43] Moritz Vandenheert, Sonia Laguna, Ricards Marcinkevics, and Julia E. Vogt. Stochastic concept bottleneck models. *ArXiv*, abs/2406.19272, 2024. 2
- [44] C. Wah, S. Branson, P. Welinder, P. Perona, and S. Belongie. Caltech-ucsd-birds-200-2011. Technical Report CNS-TR-2011-001, California Institute of Technology, 2011. 4
- [45] Jamelle Watson-Daniels, David C Parkes, and Berk Ustun. Predictive multiplicity in probabilistic classification. In *Proceedings of the AAAI Conference on Artificial Intelligence*, pages 10306–10314, 2023. 2
- [46] Jiaqi Wu, Junbiao Pang, and Qingming Huang. Decorrelating structure via adapters makes ensemble learning practical for semi-supervised learning. *arXiv preprint arXiv:2408.04150*, 2024. 3
- [47] Yongqin Xian, Christoph H. Lampert, Bernt Schiele, and Zeynep Akata. Zero-shot learning—a comprehensive evaluation of the good, the bad and the ugly. *IEEE Transactions on Pattern Analysis and Machine Intelligence*, 41(9):2251–2265, 2019. 4
- [48] Rui Xin, Chudi Zhong, Zhi Chen, Takuya Takagi, Margo Seltzer, and Cynthia Rudin. Exploring the whole rashomon set of sparse decision trees. *Advances in neural information processing systems*, 35:14071–14084, 2022. 1, 2
- [49] Xin-Chao Xu, Yi Qin, Lu Mi, Hao Wang, and Xiaomeng Li. Energy-based concept bottleneck models: Unifying prediction, concept intervention, and probabilistic interpretations. In *International Conference on Learning Representations*, 2024. 2
- [50] Shaofeng Zhang, Meng Liu, and Junchi Yan. The diversified ensemble neural network. In *Proceedings of the 34th Conference on Neural Information Processing Systems (NeurIPS)*, Red Hook, NY, USA, 2020. Curran Associates Inc. 2, 3, 5
- [51] Chudi Zhong, Zhi Chen, Jiachang Liu, Margo Seltzer, and Cynthia Rudin. Exploring and interacting with the set of good sparse generalized additive models. In *Neural Information Processing Systems (NeurIPS)*, 2023. 1, 2

## Appendix

### A. Additional results comparing Rashomon CBMs to baselines

In this section, we provide more results on model performance comparison.

#### A.1. Performance of Rashomon CBMs and baselines with ViT instantiation on different datasets

The experimental setup is identical to that described in Section 4.1. For all ViT experiments, we adopt pretrained ViT-S/16 as the backbone. We instantiate our proposed framework using LoRA adapters. Each LoRA module is inserted into the  $Q$ ,  $K$ ,  $V$ , and projection matrices of every attention block, with a rank of  $r = 8$ , scaling factor  $\alpha = 16$ , and 0.1 dropout ratio. All backbones are frozen, and only the adapter parameters and concept heads are updated during training. Models are trained using the Adam optimizer with a learning rate of  $1 \times 10^{-4}$ , batch size of 64, and no weight decay for 500 epochs. We stop training early if the validation loss doesn't decrease for 30 epochs. For most datasets,  $\lambda = 1$  yields stable accuracy and diversity. For the CUB dataset, it is set to 4 to ensure diversity. Training is performed on a single NVIDIA L40 GPU (48GB) for all ViT results. For all methods, the concept predictor  $\{h_{m,j}\}_{j=1}^p$  and label classifier  $f_m$  are implemented as linear layers.

We report performance of our method and baselines based on ViT backbone on CIFAR-10 and AWA2 dataset in Table 1 and on CUB and CelebA in Table 4. Across both the CUB and CelebA datasets, Rashomon CBMs match or outperform the baselines in both task and concept accuracy. They also consistently show the lowest SHAP similarity and low concept CKA, and achieve a larger union size on CUB, indicating that the models rely on different concept representations than the baselines. On CelebA, however, the task accuracy of all baselines is lower than other datasets, despite concept accuracy being around 90% for most models (which is also partly a reflection of high number of classes). With only six available concepts, the space of concept-based explanations is intrinsically limited. Indeed, all baselines achieve a union size of exactly six, meaning that models within slices and ensembles rely on the same full set of concepts. This suggests that, for CelebA, there is might be no diversity in which concepts are used, and the observed differences across methods primarily reflect how the concepts are weighted rather than which concepts are selected. Additionally, Figure 12 visualizes the task accuracy vs. SHAP diversity ( $1 - \text{SHAP similarity}$ ) for different methods across four datasets. Overall, these results suggest that our method produces models that use concepts in more diverse ways while maintaining strong accuracy.

Table 5 shows the memory usage and number of trainable parameters for each method across all datasets when for the ViT backbone. Rashomon CBMs keep the trainable parameter count in the 2.3M – 3.0M range, which is only about 1.3% of the baseline with the largest number of parameters. Their memory usages are also the lowest among all methods and remain substantially below that of random initialization and x2c. Together with the strong accuracy and diversity results reported earlier, these findings show that Rashomon CBMs with the ViT backbone achieve accuracy, diversity, and efficiency in both memory and trainable parameters simultaneously.

	Metric	random init	dropout	c2y	x2c	Rashomon CBMs (Ours)
CUB	concept acc $\uparrow$	0.9023 $\pm$ 0.0011	0.8932 $\pm$ 0.0007	<b>0.9024 <math>\pm</math> 0.0009</b>	0.8985 $\pm$ 0.0008	0.8998 $\pm$ 0.0012
	task acc $\uparrow$	0.8302 $\pm$ 0.0069	0.7580 $\pm$ 0.0140	0.7994 $\pm$ 0.0068	0.7930 $\pm$ 0.0089	<b>0.8419 <math>\pm</math> 0.0047</b>
	pred hamming $\uparrow$	0.1549 $\pm$ 0.0046	0.1571 $\pm$ 0.0064	0.1045 $\pm$ 0.0048	<b>0.2024 <math>\pm</math> 0.0119</b>	0.1245 $\pm$ 0.0043
	concept cka $\downarrow$	0.6216 $\pm$ 0.0109	0.9085 $\pm$ 0.0076	-	<b>0.4698 <math>\pm</math> 0.0203</b>	0.6416 $\pm$ 0.0685
	SHAP sim $\downarrow$	0.9624 $\pm$ 0.0059	0.9993 $\pm$ 0.0001	0.9944 $\pm$ 0.0010	0.6256 $\pm$ 0.0615	<b>0.5190 <math>\pm</math> 0.0888</b>
	union size $\uparrow$	51	16	23	58	<b>66</b>
CelebA	concept acc $\uparrow$	0.8997 $\pm$ 0.0012	0.9019 $\pm$ 0.0010	0.9047 $\pm$ 0.0010	0.8896 $\pm$ 0.0013	<b>0.9072 <math>\pm</math> 0.0011</b>
	task acc $\uparrow$	0.4478 $\pm$ 0.0035	0.4591 $\pm$ 0.0022	0.4098 $\pm$ 0.0027	0.4412 $\pm$ 0.0035	<b>0.4799 <math>\pm</math> 0.0043</b>
	pred hamming $\uparrow$	0.3370 $\pm$ 0.0089	0.1767 $\pm$ 0.0064	0.2498 $\pm$ 0.0225	<b>0.3457 <math>\pm</math> 0.0137</b>	0.2426 $\pm$ 0.0064
	concept cka $\downarrow$	0.2141 $\pm$ 0.0248	<b>0.1559 <math>\pm</math> 0.0058</b>	-	0.2691 $\pm$ 0.0421	0.1945 $\pm$ 0.0415
	SHAP sim $\downarrow$	0.9611 $\pm$ 0.0265	1.0000 $\pm$ 0.0000	0.9878 $\pm$ 0.0107	0.9064 $\pm$ 0.0479	<b>0.8732 <math>\pm</math> 0.0919</b>
	union size $\uparrow$	6	6	6	6	6

Table 4. Comparison of Rashomon CBMs and baseline methods on the CUB and CelebA datasets using the ViT backbone. All methods achieve comparable concept and task accuracies on the test set. Our method consistently achieves better concept representation and SHAP diversity than baselines, and performs on par with or better than x2c, indicating that Rashomon CBMs effectively find diverse yet well-performing models. Best results per metric are highlighted in bold.

	Method	Mem (GiB) ↓	Mem ratio (%) ↓	Params (M) ↓	Param ratio (%) ↓
CUB	random init	36.01	-	217.3	-
	dropout	4.15	11.5%	21.8	10.0%
	c2y	3.75	10.4%	21.9	10.1%
	x2c	37.09	103.0%	217.3	100.0%
	Ours	<b>2.81</b>	<b>7.8%</b>	<b>2.9</b>	<b>1.3%</b>
CIFAR-10	random init	37.09	-	217.2	-
	dropout	4.16	11.2%	21.8	10.0%
	c2y	3.75	10.1%	21.7	10.0%
	x2c	37.09	100.0%	217.2	100.0%
	Ours	<b>2.81</b>	<b>7.6%</b>	<b>2.9</b>	<b>1.3%</b>
Awa2	random init	37.09	-	217.0	-
	dropout	4.16	11.2%	21.7	10.0%
	c2y	4.66	12.5%	21.7	10.0%
	x2c	37.09	100.0%	217.0	100.0%
	Ours	<b>2.81</b>	<b>7.6%</b>	<b>2.7</b>	<b>1.2%</b>
CelebA	random init	37.09	-	216.7	-
	dropout	4.16	11.2%	21.7	10.0%
	c2y	3.75	10.1%	21.7	10.0%
	x2c	37.09	100.0%	216.7	100.0%
	Ours	<b>2.80</b>	<b>7.6%</b>	<b>2.3</b>	<b>1.1%</b>

Table 5. Exact memory and parameter costs of different methods and their ratios relative to the random initialization across four datasets using the ViT backbone. Our method achieves strong diversity with substantially lower memory and parameter cost than baselines. Lower is better for all metrics.

## A.2. Performance of Rashomon CBMs and baselines with ResNet-18 instantiation on different datasets

For all ResNet-18 experiments, we adopt pretrained ResNet-18 as the backbone. We instantiate our proposed framework using Conv-adapters. Each Conv-Adapter module is inserted in parallel into each convolutional layer inside ResNet-18. All backbones are frozen, and only the adapter parameters and concept heads are updated during training. Models are trained using the Adam optimizer with a learning rate of  $1 \times 10^{-4}$ , batch size of 64, and no weight decay for 500 epochs. We stop training early if the validation loss doesn’t decrease for 30 epochs. In particular, we increase the learning rate to  $5 \times 10^{-3}$  when training on the CUB dataset. In addition to the four baselines introduced in Section 4.1, we include an additional lightweight but powerful baseline for the ResNet-18 backbone, which we refer to as *Partialx2c*. It is similar to the x2c baseline, but enables each model to share the same frozen backbone  $B$ . Instead of operating inside the backbone as Rashomon CBM does, *Partialx2c* inserts a model-specific residual adapter  $A_m$  for each model  $m$  between  $B$  and concept predictor  $\{h_{m,j}\}_{j=1}^p$ . This structure makes *Partialx2c* both parameter-efficient and flexible.

Table 6 provides detailed results for the ResNet-18 instantiation on CIFAR-10, Awa2, CUB, and CelebA datasets. On CIFAR-10 and Awa2 datasets, Rashomon CBMs achieve task accuracy that is competitive with or better than the baselines, with a moderate decrease in concept accuracy compared to c2y and *partialx2c*. On CUB and CelebA datasets, Rashomon CBMs have the best or near-best task accuracy, and their concept accuracy remains close to that of the best baselines.

Meanwhile, Rashomon CBMs can achieve better diversity than most baselines. On the Awa2 and CUB datasets, Rashomon CBMs achieve the lowest SHAP similarity, outperforming x2c and *partialx2c* and comparable union sizes. On the CIFAR-10 dataset, the SHAP similarity and union size obtained by Rashomon CBMs are similar to those of x2c and *partialx2c*. On the CelebA dataset, Rashomon CBMs achieve the lowest concept CKA and SHAP similarity, indicating that they learn the most distinct concept representations. Figure 13 visualizes the task accuracy vs. SHAP diversity for different methods across four datasets. Overall, the ResNet-18 results align closely with those observed for the ViT backbone: Rashomon CBMs find different-yet well-performing models, capturing more diverse concept representations than the baselines while maintaining strong task accuracy.

	Metric	c2y	x2c	Random init	Dropout	Partialx2c	Rashomon CBMs (Ours)
CIFAR-10	concept acc $\uparrow$	<b>0.8813 <math>\pm</math> 0.0009</b>	0.8798 $\pm$ 0.0007	<b>0.8813 <math>\pm</math> 0.0007</b>	0.8772 $\pm$ 0.0008	0.8792 $\pm$ 0.0006	0.8669 $\pm$ 0.0004
	task acc $\uparrow$	0.9586 $\pm$ 0.0033	<b>0.9621 <math>\pm</math> 0.0012</b>	0.9585 $\pm$ 0.0021	0.9467 $\pm$ 0.0010	0.9577 $\pm$ 0.0032	0.9444 $\pm$ 0.0019
	pred hamming $\uparrow$	0.0085 $\pm$ 0.0008	0.0315 $\pm$ 0.0011	<b>0.0386 <math>\pm</math> 0.0034</b>	0.0173 $\pm$ 0.0007	0.0068 $\pm$ 0.0007	0.0218 $\pm$ 0.0013
	concept cka $\downarrow$	—	<b>0.3157 <math>\pm</math> 0.2543</b>	0.8632 $\pm$ 0.0107	1.0000 $\pm$ 0.0000	0.6531 $\pm$ 0.2273	0.5340 $\pm$ 0.1965
	SHAP sim $\downarrow$	0.9119 $\pm$ 0.0226	<b>0.0677 <math>\pm</math> 0.0354</b>	0.8597 $\pm$ 0.0184	0.9938 $\pm$ 0.0007	0.1013 $\pm$ 0.0500	0.1028 $\pm$ 0.0606
	union size $\uparrow$	21	<b>58</b>	30	15	50	54
AwA2	concept acc $\uparrow$	0.9746 $\pm$ 0.0013	0.9763 $\pm$ 0.0008	0.9692 $\pm$ 0.0009	0.9629 $\pm$ 0.0014	<b>0.9788 <math>\pm</math> 0.0014</b>	0.9508 $\pm$ 0.005
	task acc $\uparrow$	0.9001 $\pm$ 0.0084	0.9096 $\pm$ 0.0041	0.9007 $\pm$ 0.0061	0.8896 $\pm$ 0.0061	0.9182 $\pm$ 0.0079	<b>0.9192 <math>\pm</math> 0.0048</b>
	pred hamming $\uparrow$	0.0359 $\pm$ 0.0018	0.0790 $\pm$ 0.0021	<b>0.0923 <math>\pm</math> 0.0055</b>	0.0347 $\pm$ 0.0015	0.0221 $\pm$ 0.0012	0.0463 $\pm$ 0.0026
	concept cka $\downarrow$	-	<b>0.3490 <math>\pm</math> 0.1057</b>	0.9238 $\pm$ 0.0079	1.0000 $\pm$ 0.0000	0.7510 $\pm$ 0.1307	0.6742 $\pm$ 0.1746
	SHAP sim $\downarrow$	0.9765 $\pm$ 0.0037	0.1303 $\pm$ 0.0575	0.9547 $\pm$ 0.0062	0.9992 $\pm$ 0.0001	0.4108 $\pm$ 0.1226	<b>0.1119 <math>\pm</math> 0.0842</b>
	union size $\uparrow$	26	<b>63</b>	41	10	62	58
CUB	concept acc $\uparrow$	<b>0.9027 <math>\pm</math> 0.0012</b>	0.8983 $\pm$ 0.0009	0.9013 $\pm$ 0.0007	0.8936 $\pm$ 0.0010	0.8571 $\pm$ 0.0007	0.8876 $\pm$ 0.0011
	task acc $\uparrow$	0.6731 $\pm$ 0.0113	0.6993 $\pm$ 0.0056	0.6945 $\pm$ 0.0061	0.6606 $\pm$ 0.0199	0.6796 $\pm$ 0.0054	<b>0.6996 <math>\pm</math> 0.0091</b>
	pred hamming $\uparrow$	0.2234 $\pm$ 0.0072	0.3152 $\pm$ 0.0061	<b>0.3175 <math>\pm</math> 0.0060</b>	0.1258 $\pm$ 0.0043	0.1959 $\pm$ 0.0050	0.2571 $\pm$ 0.0060
	concept cka $\downarrow$	—	<b>0.4888 <math>\pm</math> 0.0226</b>	0.6095 $\pm$ 0.0120	0.9703 $\pm$ 0.0009	0.9562 $\pm$ 0.0048	0.6561 $\pm$ 0.0805
	SHAP sim $\downarrow$	0.9934 $\pm$ 0.0010	0.6607 $\pm$ 0.0487	0.9443 $\pm$ 0.0090	0.9993 $\pm$ 0.0001	0.8783 $\pm$ 0.0138	<b>0.3371 <math>\pm</math> 0.0728</b>
	union size $\uparrow$	21	59	50	14	<b>61</b>	59
CelebA	concept acc $\uparrow$	0.9042 $\pm$ 0.0006	0.8826 $\pm$ 0.0008	0.9013 $\pm$ 0.0012	<b>0.9056 <math>\pm</math> 0.0010</b>	0.8803 $\pm$ 0.0012	0.8995 $\pm$ 0.0012
	task acc $\uparrow$	0.4168 $\pm$ 0.0005	0.4482 $\pm$ 0.0019	0.4489 $\pm$ 0.0035	<b>0.4557 <math>\pm</math> 0.0046</b>	0.4381 $\pm$ 0.0025	0.4556 $\pm$ 0.0018
	pred hamming $\uparrow$	0.2400 $\pm$ 0.0172	0.3433 $\pm$ 0.0117	<b>0.3526 <math>\pm</math> 0.0088</b>	0.1111 $\pm$ 0.0072	0.2584 $\pm$ 0.0099	0.2382 $\pm$ 0.0108
	concept cka $\downarrow$	—	0.3003 $\pm$ 0.0433	0.2831 $\pm$ 0.0300	0.3657 $\pm$ 0.0185	0.4050 $\pm$ 0.0174	<b>0.2793 <math>\pm</math> 0.051</b>
	SHAP sim $\downarrow$	0.9762 $\pm$ 0.0202	0.9172 $\pm$ 0.0428	0.9638 $\pm$ 0.0277	1.0000 $\pm$ 0.0000	0.9274 $\pm$ 0.0421	<b>0.8989 <math>\pm</math> 0.0649</b>
	union size $\uparrow$	6	6	6	6	6	6

Table 6. Comparison of Rashomon CBMs and baseline methods on the CIFAR-10, AwA2, CUB, and CelebA datasets using the ResNet-18 backbone. All methods achieve comparable concept and task accuracies on the test set. Our method in general achieves better concept representation and SHAP diversity than the baselines, and performs on par with or better than x2c, indicating that Rashomon CBMs effectively find diverse yet well-performing models. Best results per metric are highlighted in bold.

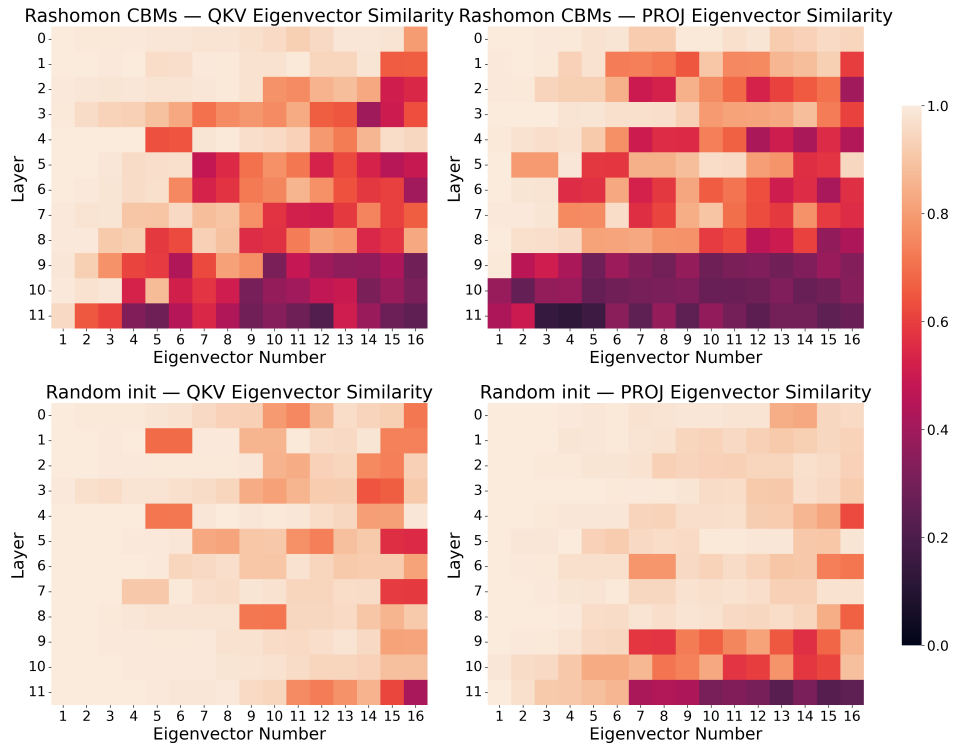
## B. Additional layer-wise ablation study

### B.1. Additional layer-wise ablation study for the ViT instantiation

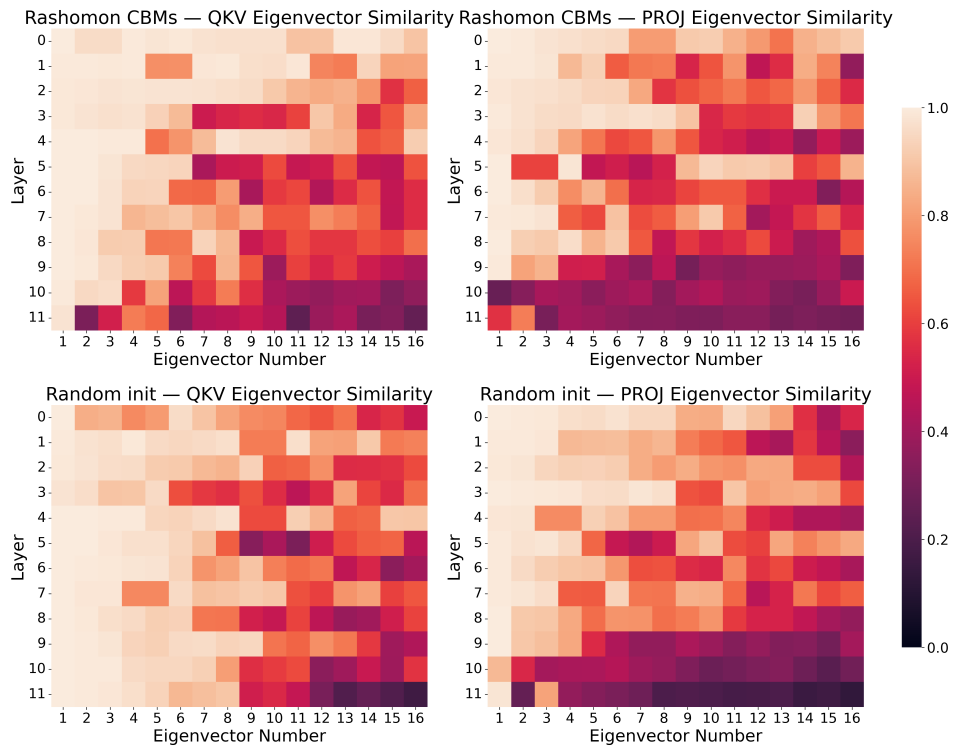
In Section 4.5, we compare the layer-wise eigenvector similarity of the QKV and projection matrices between models on AwA2. Figures 6a and 6b provide extra visualizations for Rashomon CBMs (top) and the baseline with random initialization (bottom) on AwA2 dataset and CIFAR-10 dataset respectively. Across both datasets and both QKV and projection matrices, for Rashomon CBMs we observe a clear pattern: similarity decreases noticeably with depth, and within each layer the later eigenvectors show lower similarity than the leading ones. This indicates that Rashomon models share similar low-level representations but diverge increasingly in deeper layers. This structured reduction in similarity reflects the effect of our method in encouraging meaningful representational diversity by using the adapter modules.

We also include the results for the random-init baseline (see bottom subfigures in Figures 6a and 6b). Its behavior differs across datasets. On AwA2, models obtained from different random initializations remain highly similar across most layers with only a small reduction toward the deepest layers. On CIFAR-10, random-init exhibits lower similarity overall but the depth-dependent decrease is less evident for the QKV matrices. This suggests that training from random initialization without additional structure may be more sensitive to dataset characteristics

We further explore where diversity emerges through a layerwise ablation study on the CUB dataset. Following the setup in Section 4.5, we start from a configuration where all models share the same adapter in every layer, and then force independent adapters at a single layer while keeping the rest shared. We measure concept similarity, concept CKA, SHAP similarity, and task and concept accuracy. As shown in Figure 7, similarity remains high across metrics since the adapters are shared in most layers. Concept CKA has a slight decreasing trend when independence is introduced in deeper layers, suggesting that later layers are likely to contribute more to concept-level diversity. SHAP similarity remains quite stable across layers and does not display a clear monotonic trend. Concept accuracy and task accuracy show small fluctuations across different configurations.



(a) Layerwise eigenvector similarity for Rashomon CBM (top) and random initialization (bottom) with ViT backbone on AwA2 dataset.



(b) Layerwise eigenvector similarity for Rashomon CBM (top) and random initialization (bottom) with ViT backbone on CIFAR-10 dataset.

Figure 6. Layerwise eigenvector similarity calculated on the QKV matrices and projection matrices. Rashomon CBMs show a clear decrease in similarity in deeper layers on both datasets.

## B.2. Layer-wise ablation study for the ResNet-18 instantiation

We perform a similar layer-wise ablation study using a ResNet-18 backbone. In our original setup, each convolutional layer in ResNet-18 has  $M$  parallel adapters, one for each model. In this ablation, we share adapters across all models for every convolutional layer in most blocks, and introduce independent adapters for each model only within the convolutional layers of a selected block. Figures 14 report concept similarity, concept CKA, SHAP similarity, and the corresponding accuracy metrics as we move the independent Conv-adapters from shallow to deeper layers on the CIFAR-10 dataset.

On CIFAR-10, concept CKA exhibits a clear decreasing trend as the independent adapters are placed in the deeper layers in the network. Concept similarity and SHAP similarity remain low across all configurations, and their error bars largely overlap. Concept and task accuracies are quite stable.

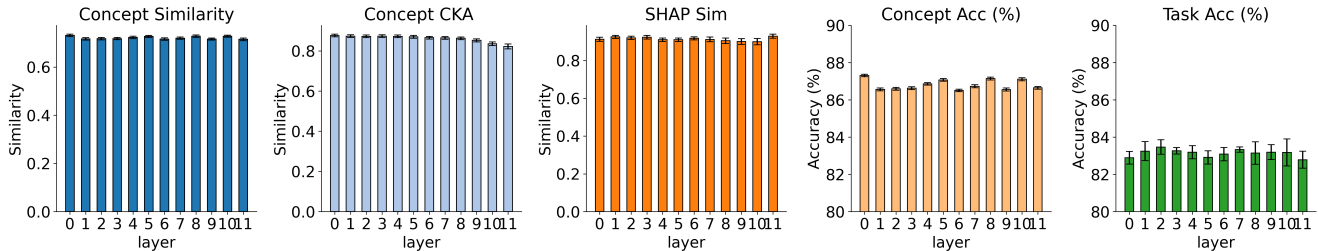


Figure 7. Layerwise ablation analysis on the CUB dataset with the ViT backbone. We switch the adapters in each layer from shared to independent one at a time. Task accuracy shows small fluctuations across different configurations, but remains within error bar range. Concept diversity is quite stable across all metrics, with a slight decreasing trend in concept CKA.

## C. Additional Scalability Experiments

In this section, we report additional results on how the size of the Rashomon slice influences performance on the CUB dataset. Using the same setup as in Section 4.4, we vary the number of models from  $M = 10$  to  $M = 25$  and track both accuracy and diversity. As shown in Figure 8, as  $M$  increases, concept similarity (based on cosine similarity) decreases as  $M$  increases, indicating that the concept representations across models become less aligned. In contrast, concept CKA increases with larger Rashomon slice sizes, suggesting that while the representations differ in cosine similarity, they still capture similar concept-level information. SHAP similarity remains relatively stable across all values of  $M$  but has large error bars. Concept accuracy decreases slightly with larger  $M$ , while task accuracy stays stable. Together with the CIFAR-10 results, these findings show that Rashomon CBMs can be expanded to larger slice sizes without decreasing predictive accuracy. The diversity metrics are related to the intrinsic variability of the dataset. When deciding the slice size, one may want to take into consideration how much diversity the data appears to support, as increasing the size of the Rashomon slice beyond that could introduce variation that is less meaningful.

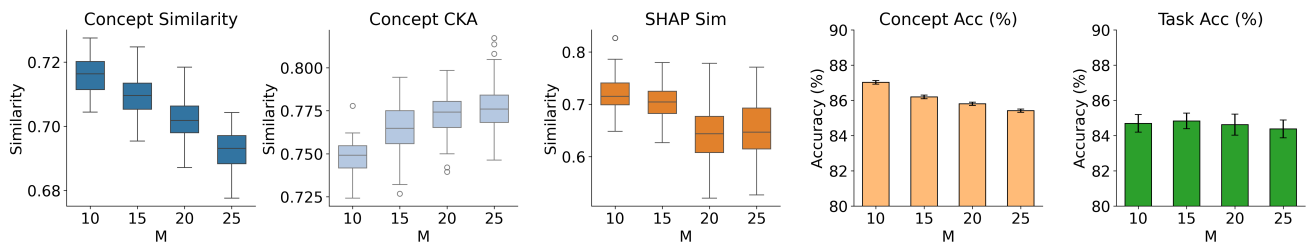


Figure 8. Effect of varying the number of models ( $M$ ) from 10 to 25 on accuracy and diversity on the CUB dataset. As  $M$  increases, concept similarity decreases while concept CKA increases. Task accuracy stays stable while concept accuracy decreases slightly.

## D. Additional Qualitative Analysis

In this section, we provide additional qualitative analysis both on the Awa2 and CUB datasets.

Figure 9 includes visualization of all 10 models for the tiger class case study we showed in Section 4.6. We selected models 0, 3, 7, 8, and 9 (out of the 10 total models) for Section 4.6 because they exhibit the most informative and diverse

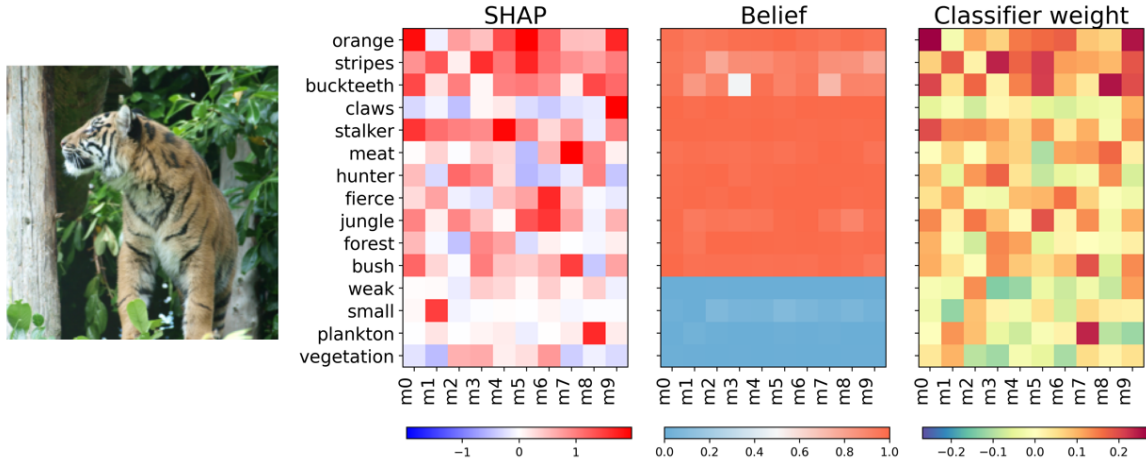


Figure 9. Qualitative Analysis of Rashomon CBMs on a tiger image from Awa2 dataset (this figure is an extension of Figure 5). The left heatmap shows sparse SHAP importance for all 10 models, indicating each model relies on different concepts for prediction. The middle heatmap shows the predicted concept probabilities, which are quite consistent across models. The right heatmap visualizes the linear classifier weights assigned to each concept, suggesting that the models differ in how they map concepts to final predictions.

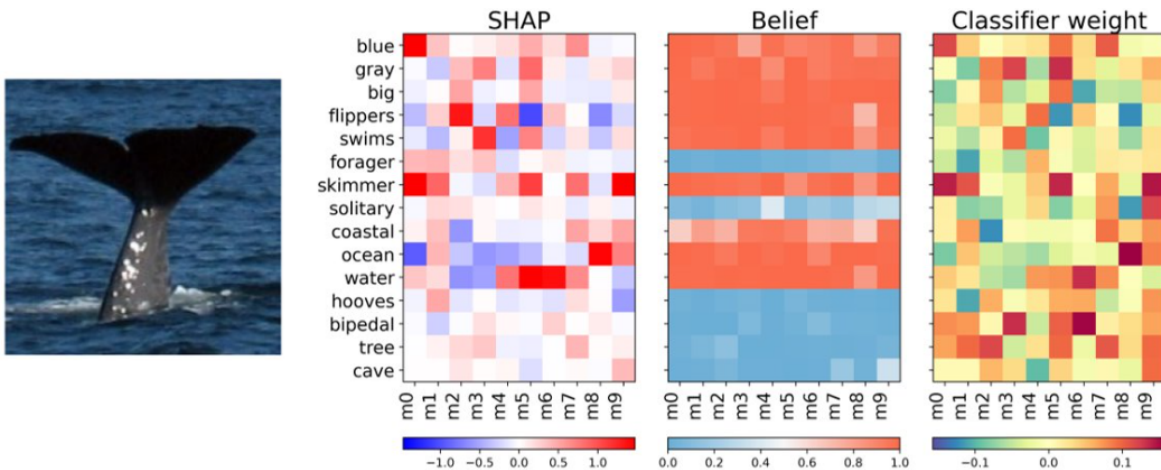


Figure 10. Qualitative Analysis of Rashomon CBMs on a blue whale image from Awa2 dataset. The left heatmap shows SHAP importance for all 10 models. The middle heatmap shows the predicted concept probabilities. The right heatmap visualizes the linear classifier weights assigned to each concept. Overall beliefs are quite consistent across models with observable diversity in models based on SHAP and classifier weights heatmaps.

patterns of concept usage. Other, non-selected, models still rely on different and reasonable concepts. For example, model 1 has strong reliance on “stripes” and “stalker”.

We provide a similar use case study for an input from the blue whale class from the Awa2 dataset in Figure 10. From this blue whale example, we observe sparse SHAP activation and consistent beliefs, indicating that Rashomon CBMs can be accurate and diverse. We also observe that models learn in different ways. For instance, model 9 mainly learns behavioral concepts, highlighting “skimmer” and “solitary” in classifier weights. In contrast, model 5 learns from the visual traits such as “blue”, “big” and “gray”. We also observe some models mainly uses environmental, spurious concepts, such as “ocean” (e.g. model 8).

We also provide a qualitative visualization of Lazuli Bunting from the CUB dataset. Here, we picked the concepts based on the high belief and, as a result, the concepts mainly focus on color traits, which are the most prominent characteristics of Lazuli Bunting. Our qualitative analysis shows that models exhibit mixed agreement in their beliefs: all of them reliably detect some traits of Lazuli Bunting like “blue primary color” and “shorter than head bill length”, while others concepts like

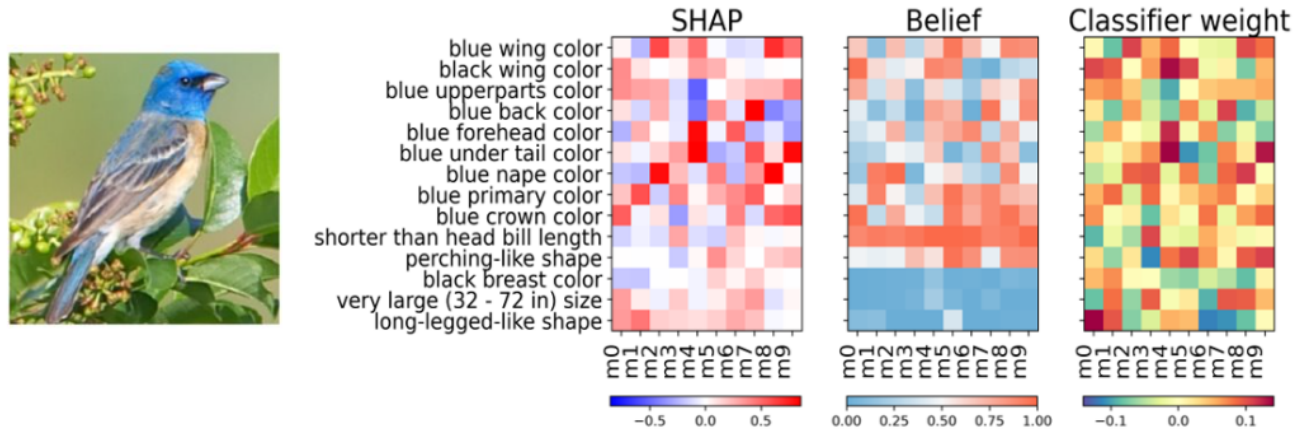


Figure 11. Qualitative Analysis of Rashomon CBMs on a Lazuli Bunting image from CUB dataset. The left heatmap shows SHAP importance for all 10 models. The middle heatmap shows the predicted concept probabilities. The right heatmap visualizes the linear classifier weights assigned to each concept. Overall, beliefs exhibit some level of diversity, leading to models using inclusion/exclusion reasoning of visual concepts. SHAP and classifier weights heatmaps appear visually aligned, diverse, and sparse.

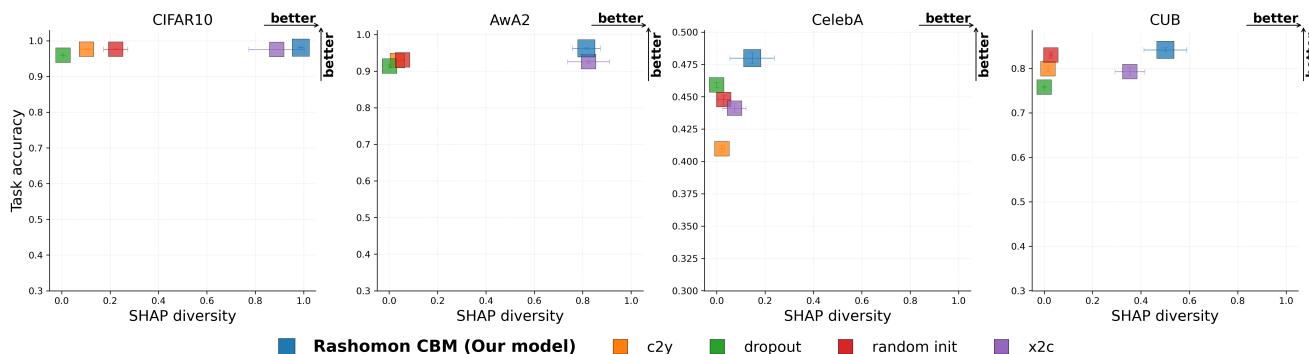


Figure 12. Task accuracy versus SHAP diversity for all methods across four datasets using the ViT backbone. Higher values on both axes indicate better performance and greater model diversity. All models achieve similar task accuracy, but Rashomon CBMs (blue) consistently exhibit substantially higher SHAP diversity than the baselines, indicating that they rely on more diverse concepts for prediction while maintaining strong accuracy.

“black wing color” have positive and negative beliefs from models. Thus, the models share a consistent perception of some important concepts, and their diversity comes from how they weigh or utilize other concepts.

We also observe that, on the CUB dataset, SHAP heatmaps track the classifier weights closely, suggesting that SHAP provides a reasonable approximation of global concept importance in this domain.

Detailed inspection of individual models highlights distinct reasoning strategies. For example, models 7 and 8 focus on disjoint local features. Model 7 is driven almost entirely by “blue back color” and “blue under tail color”, while Model 8 focuses on “blue nape color” and “blue wing color”. Model 4 focuses on fine-grained cues. It assigns a strong positive SHAP value to the specific feature “blue forehead”, while giving a negative SHAP value to the more generic “blue upperparts”. This suggests that the model suppresses broad color patterns and instead relies on precise, diagnostic markings to distinguish Lazuli Bunting from similar all-blue species.

Collectively, these models cover a range of strategies, focusing on visual appearance, specific anatomical patches, and exclusion reasoning. While this illustrates meaningful diversity within the Rashomon set, the overall range of strategies is naturally limited by the CUB dataset, which lacks environmental or contextual concepts. As a result, we observe less diversity here than on datasets such as AwA2, where models can draw on a broader set of concepts.

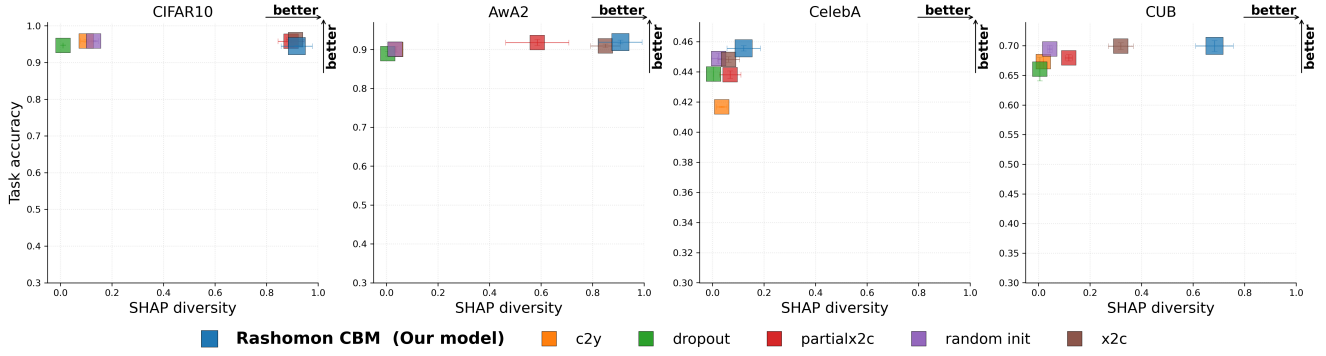


Figure 13. Task accuracy versus SHAP diversity for all methods across four datasets using the ResNet-18 backbone. Higher values on both axes indicate better performance and greater model diversity. All models achieve similar task accuracy, but Rashomon CBMs (blue) consistently exhibit substantially higher SHAP diversity than the baselines, indicating that they rely on more diverse concepts for prediction while maintaining strong accuracy.

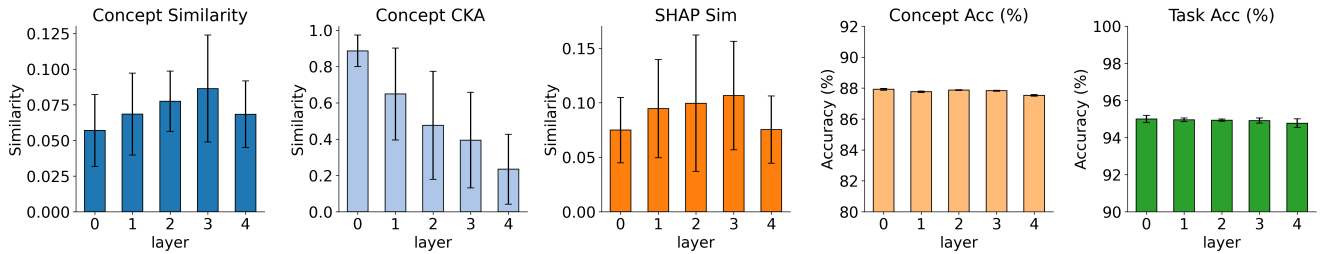


Figure 14. Layerwise ablation analysis on CIFAR-10 with a ResNet-18 backbone. Adapters in each layer are switched from shared to independent one at a time.

## E. Future Works

Rashomon CBMs opens up multiple opportunities for future research in interpretable deep learning and the Rashomon Effect. Currently, the number of models  $M$  must be specified by the user, and determining an adaptive or data-driven criterion for choosing this number remains an open question. Future research may develop automated Rashomon slice discovery methods that expand the slice until a stability or redundancy threshold is reached.

From an algorithmic standpoint, our frameworks can potentially also be applied or integrated with other novel CBM methods to include probabilistic embeddings or concept hierarchy structure. Further, loss modifications such as introducing sparsity regularization may improve the usability of the system as each model will rely on more or less concepts leading to more understandable solutions. Moreover, integrating user interfaces and visualization dashboards could make the exploration of concept diversity accessible to non-experts, leading to more transparent collaboration between model developers and domain stakeholders.